Materials Horizons

ROYAL SOCIETY OF CHEMISTRY

COMMUNICATION

View Article Online
View Journal | View Issue

Cite this: *Mater. Horiz.*, 2023, 10, 3582

Received 4th May 2023,
Accepted 5th June 2023

DOI: 10.1039/d3mh00676j

rsc.li/materials-horizons

Pioneering research on blue "hot exciton" polymers and their application in solution-processed organic light-emitting diodes†

Jiasen Zhang,[ab] Wei Li,*[ab] Lingling Lyu,[c] Qiang Wei,*[ab] Yuanyuan Meng,[ab] Deli Li,[d] Zhichuan Wang,[abe] Ming Luo,[ab] Songyu Du,[ab] Xu Xu,[c] Xiaoli Zhang,[e] Guohua Xie *[f] and Ziyi Ge *[ab]

An innovative novel category of polymeric hybridized local and charge-transfer (HLCT) blue materials prepared *via* solution processing has yet to be reported. This study introduces three polymers, namely PZ1, PZ2, and PZ3, incorporating donor–acceptor–donor (D–A–D) structures with carbazole functioning as the donor and benzophenone as the acceptor. To regulate the luminescence mechanism and conjugation length, carbonyl and alkyl chains are strategically inserted into the backbone. Theoretical calculation and transient absorption spectroscopy illustrate that the robust spin-orbit coupling between high-lying singlet excited states (S_m: $m \leqslant 4$) and triplet excited states (T_n: $n \leqslant 7$) of the polymers hastens and significantly heightens the efficiency of reverse intersystem crossing processes from T_n states. Furthermore, the existence of multiple degenerated frontier molecular orbits and significant overlaps between T_n and S_m states give rise to added radiative pathways that boost the radiative rate. This study marks a fundamental and initial manifestation of HLCT materials within the polymer field and provides a new avenue for the design of highly efficient polymeric emitters.

New concepts

The scientific community has been captivated by the phenomenal potential of hybridized local and charge-transfer (HLCT) materials, commonly referred to as "hot exciton" materials, which display an incomparable ability to achieve theoretical 100% internal quantum efficiency and low-efficiency roll-off through their rapid reverse intersystem crossing (RISC) process *via* high-lying channels. In this investigation, we have successfully synthesized a series of polymers endowed with HLCT properties, thereby marking a significant milestone in the realization of HLCT materials in the polymer arena. Key to the realization of HLCT properties for these polymers was the moderation of the electron-donating capacity of the conjugated backbone through the targeted implementation of a carbonyl unit. Furthermore, our exhaustive exploration encompassed the regulation of electron cloud distribution within the repeating unit through the electron patterning effect of the backbone carbonyl group, culminating in the demonstration of the crucial role of the electron donor capacity of the balanced donor unit in the regulation process. Interestingly, we found that PZ3 exhibited the highest level of superiority on account of the balanced electron-donating ability intrinsic to the D–A–D molecular structure.

1. Introduction

Recent research has revealed that 25% singlet and 75% triplet excitons can combine to efficiently recombine injected electrons and holes in organic light-emitting diodes (OLEDs).[1,2] Considerable endeavors have been devoted to enhancing efficiency in recent years *via* harnessing triplet excitons.[3–6] Notably, phosphorescent materials and thermally activated delayed fluorescence (TADF) materials are garnering attention as they can offer the potential of achieving unity internal quantum efficiency (IQE). These developments highlight exciting new directions in OLED research.[7–10] There are manifold imperfections impeding their progression. Relating to phosphorescent emitters, the incorporation of precious metallic elements unequivocally contributes to enhanced expenses.[11,12] Moreover, while TADF materials consist solely of organic molecules, their molecular arrangements are constrained, invariably necessitating a certain degree of highest occupied molecular orbital

[a] *Zhejiang Provincial Engineering Research Center of Energy Optoelectronic Materials and Devices, Ningbo Institute of Materials Technology and Engineering, Chinese Academy of Sciences, Ningbo, 315201, P. R. China. E-mail: liwei1987@nimte.ac.cn, weiqiang@nimte.ac.cn, geziyi@nimte.ac.cn*
[b] *Center of Materials Science and Optoelectronics Engineering, University of Chinese Academy of Sciences, Beijing, 100049, P. R. China*
[c] *Ningbo Dayang Technology Co., Ltd., Ningbo 315000, P. R. China*
[d] *State Key Laboratory of Luminescent Materials and Devices and Institute of Polymer Optoelectronic Materials and Devices, South China University of Technology, Wushan Road 381, Tianhe District, Guangzhou 510640, Guangdong Province, P. R. China*
[e] *School of Materials Science and Engineering, Zhengzhou University, Zhengzhou 450001, People's Republic of China*
[f] *Sauvage Center for Molecular Sciences, Hubei Key Lab on Organic and Polymeric Optoelectronic Materials, Department of Chemistry, Wuhan University, Wuhan 430072, P. R. China*

† Electronic supplementary information (ESI) available. See DOI: https://doi.org/10.1039/d3mh00676j

(HOMO) – lowest unoccupied molecular orbital (LUMO) separation to satisfy the prerequisite of minimal energy splitting (ΔE_{ST}) between the S_1 and T_1 states. Thus, it is worth noting that the oscillator strength and radiative rate in the S_1 state are comparatively subdued, as evidenced by previous research.[13–16] Fortunately, as an alternative, a novel mechanism which can also realize 100% IQE *via* a reverse intersystem crossing (RISC) process from the high-lying triplet (T_n) states (hRISC) to S_m states has been explored.[17,18] In contrast with the TADF mechanism, fluorescent molecules with hybridized local and charge-transfer (HLCT) state characters inherently have a large overlap between ''particle'' and ''hole'' in excited states, which undoubtedly amplifies the oscillator strength of the S_1 state.[19–21] Currently, numerous HLCT small molecules comprising donor–acceptor–donor (D–A–D) molecular configurations have been designed and reported.[22,23] However, the task of achieving blue emission through the HLCT mechanism while incorporating long conjugated chains in polymers remains a formidable challenge that is yet to be addressed in the scientific community.

In this work, three polymers named **PZ1**, **PZ2**, and **PZ3** exhibiting HLCT properties were designed and synthesized (Fig. 1). Carbazole and benzophenone were judiciously selected as the donor and acceptor moieties, respectively. Interestingly, the carbonyl group appended to the 3,6 position of the carbazole unit impacts its electron donation ability, thereby regulating the luminescence mechanism of the polymer.

Moreover, the elongated alkyl chain interposed between the two carbonyl groups facilitated the separation of the conjugated units, resulting in a blue-shifted emission, along with enhanced solubility characteristics of the molecules. Theoretical calculations have revealed that these polymers exhibit remarkably high spin-orbit coupling matrix element (SOCME) values ranging from 10–25 cm^{-1} between energetically close S_m ($m \leq 4$) and T_n ($n \leq 7$) states. This result is highly conducive to a rapid and efficient hRISC process. Moreover, the multiple degenerated frontier molecular orbits (FMOs), large overlap between T_n and S_m states, and multiple excitons transfer channels can open additional radiative pathways. All of these factors contribute to an increased hRISC and radiative rate, resulting in superior electroluminescence (EL) performance. Consequently, the doped solution-processed OLED based on **PZ3** exhibits the most exceptional performance when compared to its polymer counterparts. Furthermore, non-doped devices founded on these polymers demonstrate white emission owing to the production of an electroplex, providing a versatile avenue for achieving a single-component white OLED.

2. Results and discussion

2.1 Synthesis

The molecular structures of **PZ1–PZ3** are shown in Fig. 1, and the detailed synthetic procedure is illustrated in Scheme S1–S14 (ESI†). The monomer was prepared through Friedel–Crafts acylation reaction and nucleophilic substitution reaction, and the polymers were synthesized by Suzuki polymerization (for **PZ1** and **PZ3**) and Yamamoto polymerization (for **PZ2**). The structures of the monomer and **PZ1–PZ3** were characterized by nuclear magnetic resonance (NMR) spectroscopy. The molecular weights were monitored by time-of-flight mass spectrometer (LC-Q-TOF) and Gel permeation chromatography (GPC). It should be noted that all polymers exhibit excellent solubility, and thus they can be characterized by solution processes such as spin-coating and inkjet printing. Moreover, all the polymers show good thermal stability with a decomposition temperature (T_d, 5% weight loss) of up to 250° (Fig. S1a, ESI†). No distinct glass-transition temperature (T_g) is detected for these polymers, suggesting their amorphous character (Fig. S1b, ESI†).

2.2 Theoretical calculations

To explore the molecular properties of the polymers, the repeating units of the polymers were performed by density functional (DFT) and time-dependent density functional theory (TD-DFT) calculations (Fig. S2–S6, ESI†). The multiple degenerated frontier molecular orbits (FMOs) are energetically beneficial for accelerating the radiative rate (Fig. S2, ESI†). As shown in Fig. 2a, all these polymers demonstrate relatively large ΔE_{ST}s ($\sim$0.30 eV) between the S_1 state and T_1 state. At the same time, the ΔE_{ST}s between high-lying T_n and S_m ($m \leq 4$) are considerably small. For instance, the values between T_3 and S_m ($m \leq 2$) of **PZ1**, T_5 and S_m ($m \leq 4$) of **PZ2**, and T_7 and S_m ($m \leq 4$) of **PZ3** are considerably small, implying that the hRISC processes may occur from T_n to S_m (Tables S1 and S2, ESI†). More importantly, theoretical calculations revealed that as high as 10–25 cm^{-1} of SOCME values between S_m ($m \leq 4$) and T_n ($n \leq 7$) states are obtained for these polymers (Table S3, ESI†), which extremely gives rise to faster and more efficient hRISC. Moreover, for **PZ3**, much more energetically close

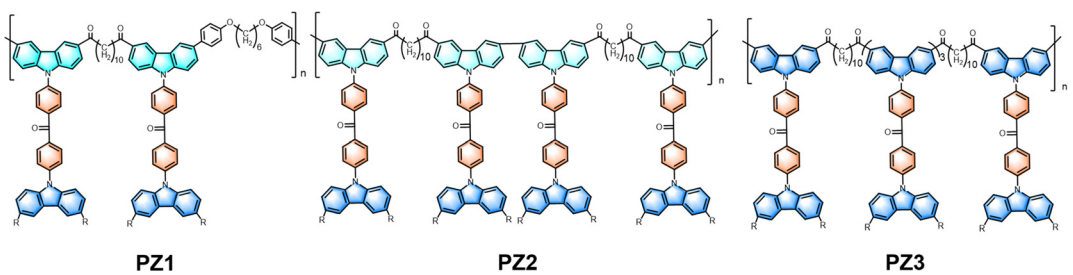

Fig. 1 Scheme of the molecular structures of **PZ1**, **PZ2** and **PZ3**, respectively. R = $C_{12}H_{25}$.

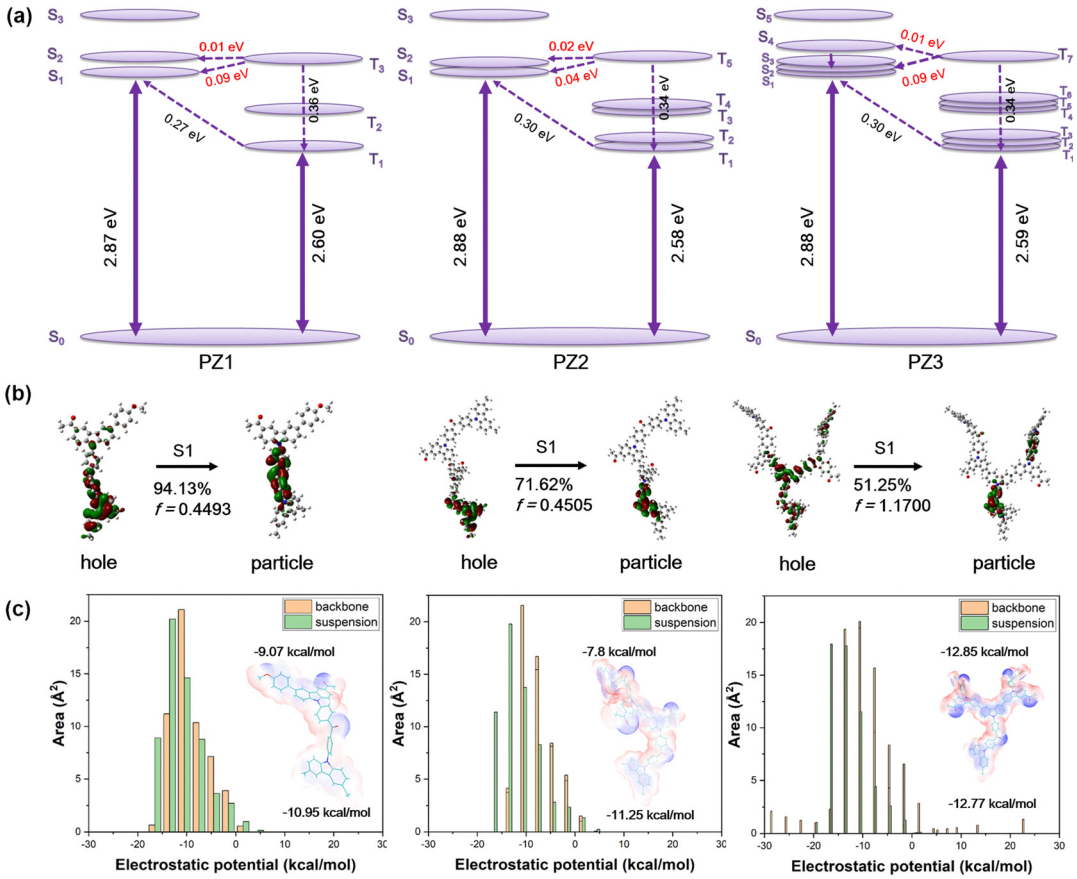

Fig. 2 (a) The calculated energy distributions. (b) The natural transition orbitals (NTOs) of $S_1 \rightarrow S_0$, and (c) the electrostatic potential (ESP) (inset: the ESP mapped molecular van der Waals surface) of the repeating units of **PZ1**, **PZ2** and **PZ3**, respectively.

S_m ($m \leq 4$) and T_n ($n \leq 7$) state energies can open an additional radiative pathway, significantly increasing the radiative rate and hRISC rate (Fig. 2a).

To further investigate the transition characteristics of the polymers, the natural transition orbital (NTO) distributions were calculated as well. As shown in Fig. 2b, in the S_m states, the "particle" was located on the benzophenone unit and the "hole" was dispersed on the suspension carbazole unit, and one benzene ring of benzophenone for **PZ1** and **PZ2** reveals that the S_1 state properties were CT state character dominant and involved little locally excited (LE) state character. For **PZ3**, the hole is located on the whole repeating unit, suggesting a typical HLCT feature. A larger hole and particle overlap were visualized for **PZ3**, showing a larger oscillator strength (f = 1.17), much higher than that of **PZ1** and **PZ2** (f = 0.45). We speculate that such a distribution may be due to the influence of the carbonyl group on the backbone chain, which reduces the electron donation capacity of the carbazole units. To prove this viewpoint, a molecular electrostatic potential (ESP) simulation was implemented (Fig. 2c).[24] The values of the backbone were higher than that of the suspension for **PZ1** (−9.07 kcal mol^{-1} *vs.* −10.95 kcal mol^{-1}) and **PZ2** (−7.80 kcal mol^{-1} *vs.* −11.25 kcal mol^{-1}), so the distribution of "hole" was more skewed towards the suspended carbazole, while as for **PZ3**, in light of the carbonyl position being far from the central carbazole unit in the backbone, the ESP of the backbone carbazole was lower than that of the suspension (−12.85 kcal mol^{-1} *vs.* −12.77 kcal mol^{-1}). Therefore, the electrostatic potential distribution in **PZ3** is higher in equilibrium compared to **PZ1** and **PZ2**, leading to a dispersive "hole" in **PZ3**. In T_n states, all the polymers exhibit distinct LE-state properties, suggesting that the T_n states are dominated by LE state properties and involve minor CT state properties. The large difference in the NTO distribution between T_n and S_m can lead to large SOCME values, as described above.

2.3 Photophysical properties

The UV-visible absorption and photoluminescence (PL) spectra of these polymers were obtained in dilute toluene solution (Fig. S7, ESI†). The high-energy absorption band at 300 nm could be attributed to the π–π* transition of the carbazole unit. A relatively weak absorption at 420 nm is ascribed to the intramolecular CT (ICT) transition from the donor to acceptor moiety (Table S4, ESI†). In the PL spectra, both **PZ1** and **PZ2** emit bright, pure blue emissions with a peak at 460 nm. In comparison, a bathochromic-shift emission is observed for **PZ3** (emission peak at 480 nm), owing to the extended conjugation of the carbazole skeleton (Table S4, ESI†). Then the dipole moment of the S_1 state was characterized by the solvatochromic experiments (Fig. 3a and Fig. S8, ESI†). In low-polarity solvents

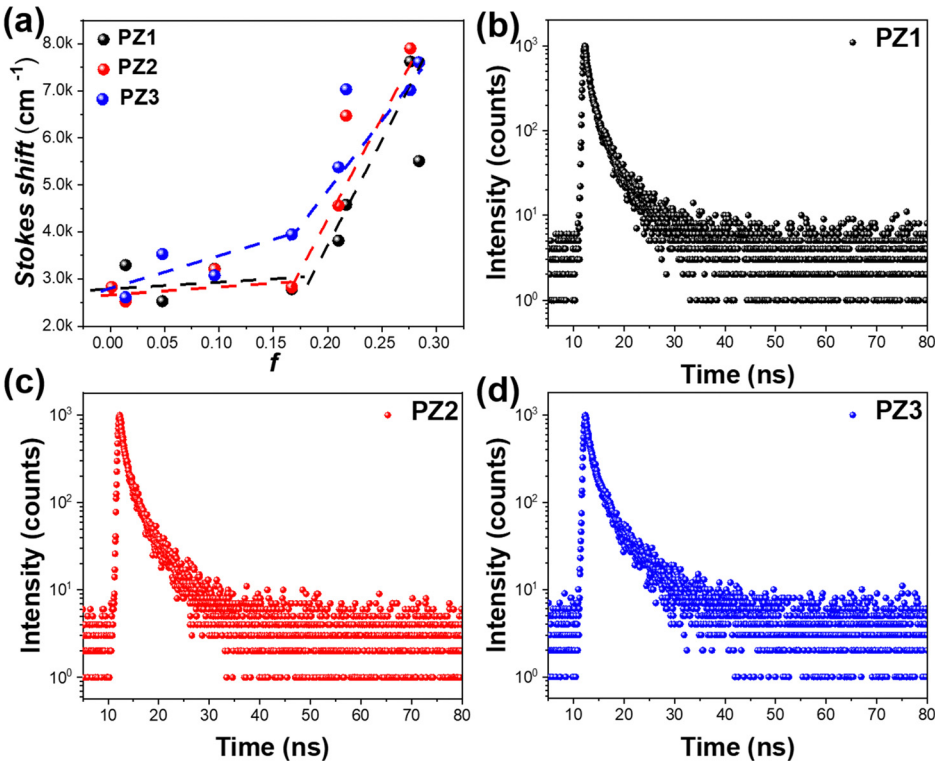

Fig. 3 (a) The Lippert–Mataga plots of the Stokes shift against the solvent polarity parameters. Transient PL decay spectra of (b) **PZ1**, (c) **PZ2** and (d) **PZ3** in mCP matrixes respectively.

($f < 0.167$), all the polymers exhibited small PL redshifts, while in high-polarity solvents ($f > 0.21$), large red-shift PL spectra were demonstrated (60 nm for **PZ1**, 50 nm for **PZ2** and 55 nm for **PZ3**). According to the Lippert–Mataga equation (Table S5, ESI†), two different linear plots were found, demonstrating their HLCT nature.

To further verify their HLCT properties, low-temperature fluorescence (PL) and phosphorescence (Pho) were carried out in neat films (Fig. S9, ESI†). According to the onsets of PL and maximum emission of Pho, their ΔE_{ST}s between the S_1 state and T_1 state were calculated to be 0.46, 0.41 and 0.43 eV, respectively, suggesting that the RISC processes from T_1 to S_1 hardly occur. Additional direct evidence comes from time-resolved PL decay spectra. As shown in Fig. 3b–d, all three polymers demonstrated a short lifetime (2–3 ns), and the delayed component was absent. In addition, the temperature-dependent

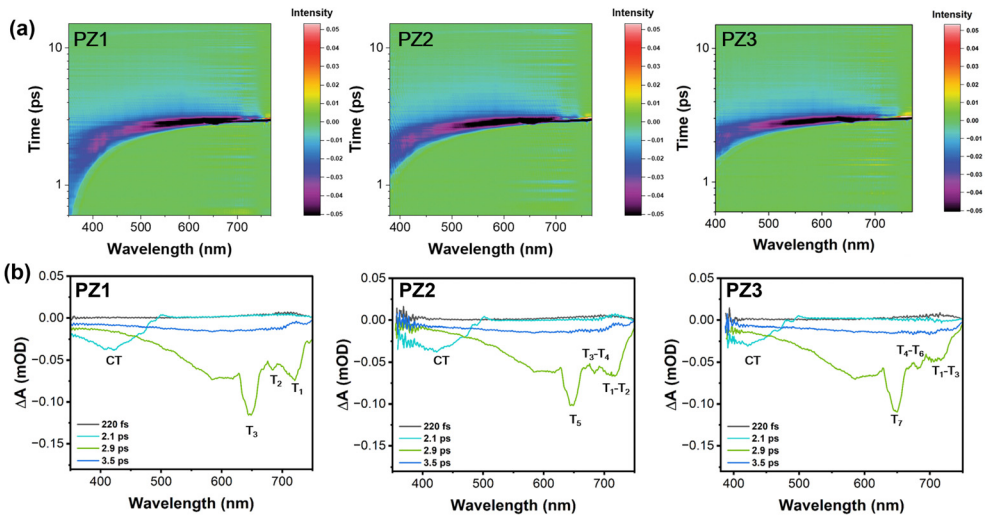

Fig. 4 (a) Contour maps of transient absorption spectra of **PZ1**, **PZ2** and **PZ3**, respectively. (b) The photoinduced absorption (PIA) signals for **PZ1**, **PZ2** and **PZ3**, respectively.

transient photoluminescence spectra of **PZ1**, **PZ2**, and **PZ3** were also performed and the curves are shown in Fig. S10 (ESI†); the nanosecond lifetimes (2–3 ns) were revealed for those polymers in the temperature-dependent transient PL spectra, excluding their TADF characters.

The exciton dynamic processes were systematically investigated by femtosecond transient absorption spectroscopy (TAS) to further explore the excited state properties.[25,26] The pump wavelength was 400 nm. The reception range was around 350–780 nm, and the polymers were dissolved in a chlorobenzene solution. As shown in Fig. 4a, the transient absorption bands from 350 to 400 nm, 380 to 400 nm, and 400 to 420 nm for **PZ1**, **PZ2** and **PZ3**, respectively, could be attributed to the S_1 state. The gradual redshift trend of the absorption bands is due to the increasing conjugation length, which is consistent with the UV-visible absorption spectra. Besides, all these polymers exhibited stronger photoinduced absorption (PIA) signals from 500 nm to 750 nm. Combined with the TD-DFT results, we can infer that the PIA signal is an absorption of the T_n states. Then, we qualitatively analyzed their excited state properties through the line graph of transient absorption (Fig. 4b). The PIA signal at ~ 420 nm can be assigned to the CT state. Moreover, there were three obvious PIA signals at 2.9 ps. The signal at 620–650 nm belonged to the higher-lying triplet states (T_3 for **PZ1**, T_5 for **PZ2** and T_7 for **PZ3**), and a weaker PIA signal at ~680 nm could be assigned to the lower excited triplet state (T_2 for **PZ1**, T_3–T_4 for **PZ2** and T_4–T_6 for **PZ3**). The signal at ~730 nm originated from the lowest excited triplet state (T_1 for **PZ1**, T_1–T_2 for **PZ2** and T_1–T_3 for **PZ3**). The absorption signal at 620–650 nm was the strongest among them, which illustrated the maximum proportion of the triplet exciton transition to this level to become "hot exciton". More interestingly, the signals representing the lowest triplet were progressively weaker from **PZ1** to **PZ3**, meaning that the number of excitons transiting to this level gradually decreased. Therefore the excitons transiting to higher triplets were increased (T_7 of **PZ3** *vs.* T_3 of **PZ1**). Hence, the exciton utilization efficiency of **PZ3** is the highest among them. In addition, the peak profile at 730 nm changes from sharp to rounded, indicating the formation of multiple close absorption signals. Then combined with the theoretical calculation, the phenomenon could be attributed to the close energy levels (T_1–T_2 of **PZ2** and T_1–T_3 of **PZ3**). This is also justified by our TAS analysis. Furthermore, the energy gap between the lowest triplet and lower triplet was ~0.13 eV according to the PIA signals at 730 nm and 680 nm. Meanwhile, the energy split between the lowest triplet and higher triplet was ~0.30 eV based on the absorption band at 620 nm, the correlation values in TD-DFT calculation were ~0.12 eV and ~0.34 eV, verifying the accuracy of the TAS analysis further.[27,28] Eventually, we could conclude that the "hot excitons" channel was established, and these materials exhibited HLCT characteristics.

2.4 OLED properties

Before preparing the device by the wet method, a scanning probe microscope (SPM) was used to evaluate the film-forming

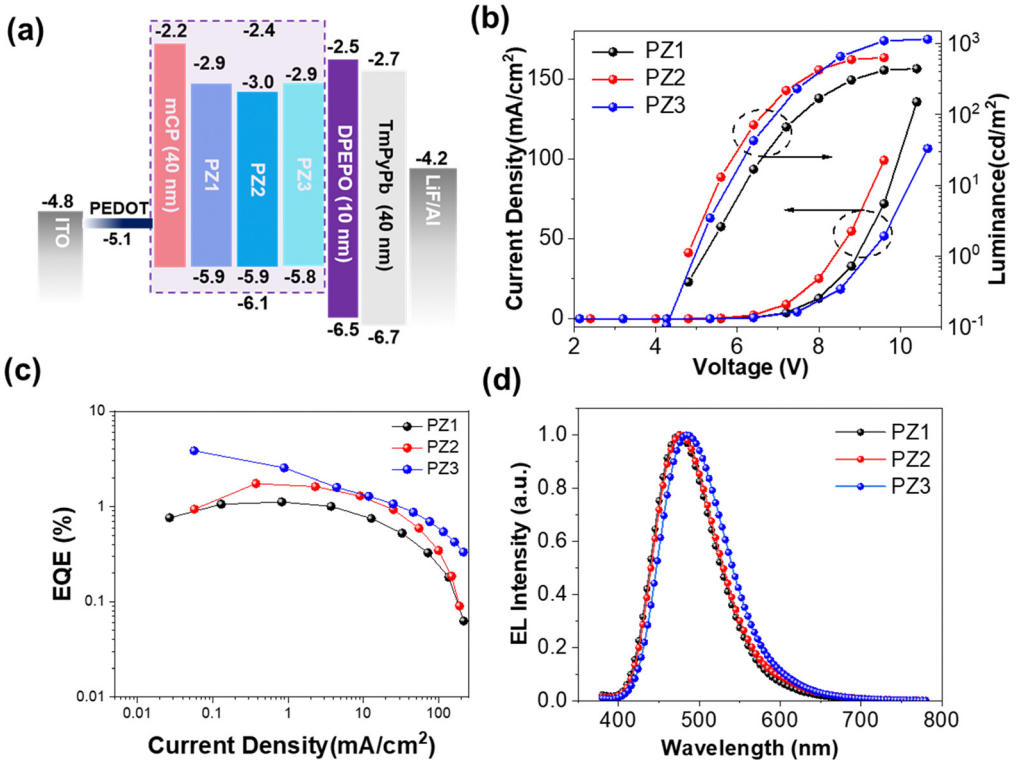

Fig. 5 (a) Device architecture and energy diagram for the solution-processed OLEDs. (b) Current density–voltage-luminance curves. (c) EQE-current density curves. (d) EL spectra.

ability, as shown in Fig. S12 (ESI†). All these polymers behaved quite smoothly with surface roughnesses of 0.29, 0.32 and 0.28 nm for PZ1, PZ2 and PZ3, respectively. Thanks to the good solubility of these polymers, solution-processed devices were fabricated with the structure of ITO/poly(3,4-ethylenedioxythiophene):poly-(styrene-sulfonic acid) (PEDOT:PSS) (30 nm)/(1,3-di(9H-carbazol-9-yl)benzene polymers (40 nm)/bis(2-(diphenylphosphino)phenyl) ether oxide (DPEPO) (10 nm)/1,3,5-tri(m-pyrid-3-yl-phenyl)benzene (TmPyPB) (50 nm)/8-hydroxyquinolinato lithium (LiF) (1 nm)/Al (100 nm), where PEDOT:PSS and LiF served as hole- and electron-injection layers, respectively. DPEPO and TmPyPB were utilized as the hole-blocking layer (HBL) and electron-transporting layer (ETL). To our surprise, all these devices exhibited white emission with the CIE coordinates of (0.32, 0.32), (0.31, 0.33) and (0.30, 0.33) and higher than 80 color rendering index (CRI) for PZ1, PZ2 and PZ3, respectively (Fig. S13, S14 and Table S6, ESI†). We assumed that it might be due to the formation of an electroplex at the interface between the emitting layer (EML) and the electron-transporting layer, since the dual-emission phenomenon was not observed in thin films under PL conditions.[29–31] To fully extract the EL pontentials of these polymers, the doped devices were fabricated, where mCP was chosen as the host material. Consequently, the OLEDs based on these polymers exhibited blue/sky-blue emissions. Correspondingly, the OLED based on PZ3 reached a maximum EQE of 3.8% (Fig. 5 and Table S7, ESI†). Such high performance can be attributed to the multiple degenerated frontier molecular orbits, large overlap between T_n and S_m states, and large SOC between the energetically close S_m and T_n states, all of which give rise to fast radiative rate and efficient hRISC, leading to high EL performance.

3. Conclusion

In this work, three blue/sky-blue polymeric emitters with D–A–D structure are designed and synthesized. They all demonstrate HLCT properties based on theoretical and experimental investigations, enabling triplet excitons to be converted to singlet excitons *via* the hRISC processes. Among them, the solution-processed OLED based on PZ3 showed the best performance among these three polymers due to the multiple degenerated frontier molecular orbits, large overlap between T_n and S_m states, and the large SOC between energetically close S_m and T_n. In addition, the non-doped devices based on these three polymers achieve white emission resulting from the formation of an electroplex. This work provides a new avenue toward blue OLEDs based on HLCT emitters and a flexible way of realizing single-component white OLEDs.

Author contributions

Jiasen Zhang: synthesized the target molecules **PZ1**, **PZ2**, and **PZ3**, carried out thermal, photophysical, and DFT calculations, and wrote and revised the manuscript; Wei Li: carried out DFT measurement, guided device preparation, and revised the initial manuscript; Qiang Wei: guided the synthesis of materials, guided essay writing, and revised the manuscript; Yuanyuan Meng: carried out the femtosecond transient absorption spectra; Deli Li: carried out the spin-orbit coupling matrix elements; Zhichuan Wang, Ming Luo, and Songyu Du: helped with the synthesis of target molecules; Lingling Lyu, Xu Xu and XiaoLi Zhang: revised the initial manuscript; Guohua Xie: optimized the device's structure, measured the device's performance, and revised the initial manuscript; Ziyi Ge: guided theory analysis, revised the initial manuscript.

Conflicts of interest

The authors declare no conflict of interest.

Acknowledgements

This work is financially supported by the National Science Fund for Distinguished Young Scholars (21925506), National Natural Science Foundation of China (U21A20331, 51773212, 81903743, and 52003088), Ningbo Key Scientific and Technological Project (2022Z124, 2022Z119), and Jiangbei District Major Science and Technology Planning Project (202102A01).

References

1 J. Zhang, Q. Wei, N. Fei, M. Zhao, L. Xie, L. Cao, X. Zhang, G. Xie, T. Wang and Z. Ge, *ACS Appl. Mater. Interfaces*, 2021, **13**, 12305–12312.
2 H. Y. Zhang, H. Y. Yang, M. Zhang, H. Lin, S. L. Tao, C. J. Zheng and X. H. Zhang, *Mater. Horiz.*, 2022, **9**, 2425–2432.
3 J. Zhang, Y. Bai, Q. Wei, L. Cao, T. Wang and Z. Ge, *J. Mater. Chem. C*, 2020, **8**, 11771–11777.
4 S. He, J. Liu, G. Yang, Z. Bin and J. You, *Mater. Horiz.*, 2022, **9**, 2818–2823.
5 X. Zheng, R. Huang, C. Zhong, G. Xie, W. Ning, M. Huang, F. Ni, F. B. Dias and C. Yang, *Adv. Sci.*, 2020, **7**, 1902087.
6 C. Lin, P. Han, S. Xiao, F. Qu, J. Yao, X. Qiao, D. Yang, Y. Dai, Q. Sun, D. Hu, A. Qin, Y. Ma, B. Z. Tang and D. Ma, *Adv. Funct. Mater.*, 2021, **31**, 2106912.
7 Y. Chen, D. Zhang, Y. Zhang, X. Zeng, T. Huang, Z. Liu, G. Li and L. Duan, *Adv. Mater.*, 2021, **33**, 2103293.
8 X. Wu, J. W. Huang, B. K. Su, S. Wang, L. Yuan, W. Q. Zheng, H. Zhang, Y. X. Zheng, W. Zhu and P. T. Chou, *Adv. Mater.*, 2021, **34**, 2105080.
9 W. Li, X. Cai, B. Li, L. Gan, Y. He, K. Liu, D. Chen, Y. C. Wu and S. J. Su, *Angew. Chem., Int. Ed.*, 2019, **58**, 582–586.
10 W. Li, B. Li, X. Cai, L. Gan, Z. Xu, W. Li, K. Liu, D. Chen and S. J. Su, *Angew. Chem., Int. Ed.*, 2019, **58**, 11301–11305.
11 J. X. Chen, K. Wang, Y. F. Xiao, C. Cao, J. H. Tan, H. Wang, X. C. Fan, J. Yu, F. X. Geng, X. H. Zhang and C. S. Lee, *Adv. Funct. Mater.*, 2021, **31**, 2101647.
12 H. J. Kim, H. Kang, J. E. Jeong, S. H. Park, C. W. Koh, C. W. Kim, H. Y. Woo, M. J. Cho, S. Park and D. H. Choi, *Adv. Funct. Mater.*, 2021, **31**, 2102588.

13 Y. F. Wang, M. Li, J. M. Teng, H. Y. Zhou and C. F. Chen, *Adv. Funct. Mater.*, 2021, **31**, 2106418.
14 X. Wang, J. Hu, J. Lv, Q. Yang, H. Tian, S. Shao, L. Wang, X. Jing and F. Wang, *Angew. Chem., Int. Ed.*, 2021, **60**, 16585–16593.
15 Y. Zheng, X. Zhu, Z. Ni, X. Wang, Z. Zhong, X. J. Feng, Z. Zhao and H. Lu, *Adv. Opt. Mater.*, 2021, **9**, 2100965.
16 Y. Zhu, S. Vela, H. Meng, C. Corminboeuf and M. Fumanal, *Adv. Opt. Mater.*, 2022, **10**, 2200509.
17 X. Guo, P. Yuan, J. Fan, X. Qiao, D. Yang, Y. Dai, Q. Sun, A. Qin, B. Z. Tang and D. Ma, *Adv. Mater.*, 2021, **33**, 2006953.
18 X. Guo, P. Yuan, X. Qiao, D. Yang, Y. Dai, Q. Sun, A. Qin, B. Z. Tang and D. Ma, *Adv. Funct. Mater.*, 2020, **30**, 1908704.
19 F. C. Kong, S. Y. Yang, X. J. Liao, Z. Q. Feng, W. S. Shen, Z. Q. Jiang, D. Y. Zhou, Y. X. Zheng and L. S. Liao, *Adv. Funct. Mater.*, 2022, **32**, 2201512.
20 S. Xiao, X. Qiao, C. Lin, Y. Li, S. Ying, J. Qin, R. Guo, L. Wang, Y. Ma and D. Ma, *Adv. Funct. Mater.*, 2022, **32**, 2207123.
21 S. Zeng, C. Xiao, J. Zhou, Q. Dong, Q. Li, J. Lim, H. Ma, J. Y. Lee, W. Zhu and Y. Wang, *Adv. Funct. Mater.*, 2022, **32**, 2113183.
22 Y. Zhang, X. Zhou, C. Zhou, Q. Su, S. Chen, J. Song and W.-Y. Wong, *J. Mater. Chem. C*, 2020, **8**, 6851–6860.
23 Z. Zhong, X. Zhu, X. Wang, Y. Zheng, S. Geng, Z. Zhou, X. J. Feng, Z. Zhao and H. Lu, *Adv. Funct. Mater.*, 2022, **32**, 2112969.
24 J. Zhang and T. Lu, *Phys. Chem. Chem. Phys.*, 2021, **23**, 20323–20328.
25 S. Manzetti and T. Lu, *J. Phys. Org. Chem.*, 2013, **26**, 473–483.
26 H. Noda, X. K. Chen, H. Nakanotani, T. Hosokai, M. Miyajima, N. Notsuka, Y. Kashima, J. L. Bredas and C. Adachi, *Nat. Mater.*, 2019, **18**, 1084–1090.
27 Y. Liu, L. Hua, S. Yan and Z. Ren, *Nano Energy*, 2020, **73**, 104800.
28 Y. Liu, L. Hua, Z. Zhao, S. Ying, Z. Ren and S. Yan, *Adv. Sci.*, 2021, **8**, 2101326.
29 X. Zhan, Z. Wu, Y. Gong, J. Tu, Y. Xie, Q. Peng, D. Ma, Q. Li and Z. Li, *Research*, 2020, 8649102.
30 L. Wen, F. Li, J. Xie, C. Wu, Y. Zheng, D. Chen, S. Xu, T. Guo, B. Qu, Z. Chen and Q. Gong, *J. Lumin.*, 2011, **131**, 2252–2254.
31 W. Song, J. Y. Lee, Y. J. Cho, H. Yu, H. Aziz and K. M. Lee, *Adv. Sci.*, 2018, **5**, 1700608.

